Clays and Clay Minerals, Vol. 57, No. 1, 72–81, 2009.

A NEW MASSIVE DEPOSIT OF ALLOPHANE RAW MATERIAL IN ECUADOR

Stephan Kaufhold[1,*], Annette Kaufhold[2], Reinhold Jahn[2], Salomón Brito[3], Reiner Dohrmann[1,4], Rainer Hoffmann[1], Hartmut Gliemann[5], Peter Weidler[5], and Manfred Frechen[6]

[1] BGR, Bundesanstalt für Geowissenschaften und Rohstoffe, Stilleweg 2, D-30655 Hannover, Germany
[2] Martin-Luther-University Halle-Wittenberg, Institute for Soil Sciences and Plant Nutrition, Weidenplan 14, D-06108 Halle, Germany
[3] SGN, Servicio Geológico Nacional, Juan León Mera y Orellana (esquina), Quito, Ecuador
[4] LBEG, Landesamt für Bergbau, Energie und Geologie, Stilleweg 2, D-30655 Hannover, Germany
[5] ITC-WGT, Abteilung Nanomineralogie, Forschungszentrum Karlsruhe, Forschungszentrum Karlsruhe GmbH, Herman-von-Helmholtz-Platz 1, D-76344 Eggenstein-Leopoldshafen, Germany
[6] GGA, Institut für Geowissenschaftliche Gemeinschaftsaufgaben, Stilleweg 2, D-30655 Hannover, Germany

Abstract—In Ecuador, DINAGE (known today as the Servicio Geológico Nacional) and the German Federal Institute for Geosciences and Natural Resources have discovered a huge allophane deposit covering an area of >4000 km^2. This study presents the results from an investigation of a 16-m thick vertical sequence from this deposit, supposedly the weathering product of two different volcanic ash deposits. In particular, the distribution of alkali metals within the uppermost layer indicates that the weathering process is still ongoing.

According to the mineralogical composition, an allophane-rich layer (allophane facies) could be distinguished from the underlying halloysite-rich layer (halloysite facies). A 2-m thick transition zone is characterized by the presence of gibbsite and intermediate specific surface area values. Only a few imogolite fibers could be identified (by scanning electron microscopy), indicating the dominance of allophane over imogolite in the allophane facies. Single allophane particles were investigated by atomic force microscopy, though this method was less accurate than transmission electron microscopy with respect to the determination of the primary particle diameter. Carbon isotope analysis (^{14}C) suggested an age of ~20,000 y for the allophane layer.

Within the allophane facies, a 4-m thick layer occurs containing 70–80 wt.% allophane with an N_2-BET specific surface area of >300 m^2/g. Based on infrared and energy-dispersive X-ray diffraction measurements, an Al/Si ratio of 1.3–1.4 was established for this allophane, which is between Al-rich and Si-rich allophane. The allophane layer may be of economic value due to the large allophane content, the small amount of organic matter, and the significant thickness of the deposit.

Key Words—AFM, Allophane, Ecuador, Nanoparticle, Special Clay.

INTRODUCTION

Allophane is known as a short-range order mineral, which mainly forms from volcanic ash. The primary particle size of allophane ranges from 3 to 5 nm (e.g. Wada, 1989). Allophane is a hydrated aluminosilicate with large specific surface area. In the late 1980s, DINAGE (known today as the SGN, Servicio Geológico Nacional) and the German Federal Institute for Geosciences and Natural Resources (BGR) explored for brick raw material in the area of Santo Domingo de los Colorados, Ecuador (Figure 1). During this campaign a deposit of allophane-rich clay was found which was not suitable for production of bricks. Detailed mineralogical investigations indicated a high proportion of allophane (Zeisig *et al.*, 2004, 2005; Kaufhold, 2007; Kaufhold *et al.*, 2007a, 2007b).

The allophane covers an area of >4000 km^2 and is generally >5 m thick. The allophane content ranges from 50 to 60 wt.%, locally up to ~80 wt.% (Dohrmann *et al.*, 2002). Samples were collected, mainly along roads, at depths of between 1 and 9 m below the surface.

The objective of the study was to characterize the allophane deposit with respect to basic material properties and mineral abundance. Allophane-rich material is of interest from an industrial point of view because of its large specific surface area (*e.g.* Yuan, 2004). Allophane mining and industrial applications in general are scarcely reported (except for Benbow, 1990, for example), probably because of the lack of high-quality allophane deposits. Important criteria for high-quality raw material are the allophane content, the thickness of the allophane layer, and the amount of organic carbon present (should be as small as possible). The Ecuadorian allophane deposit, therefore, is believed to be of potential economic value. The chemical and mineralogical characterization of the deposit are summarized.

LOCATION AND GEOLOGICAL SETTING

The allophane-bearing area discovered so far is located north and west of Santo Domingo de los

* E-mail address of corresponding author:
s.kaufhold@bgr.de
DOI: 10.1346/CCMN.2009.0570107

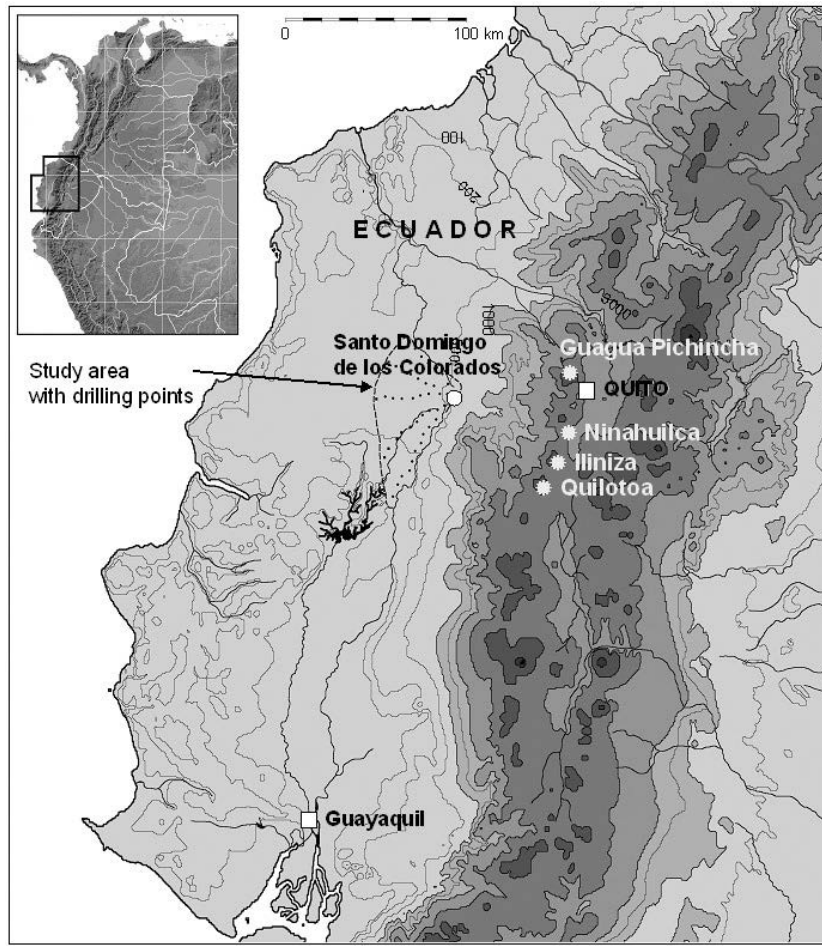

Figure 1. Map of Ecuador showing the investigated area to the west of Santo Domingo de los Colorados.

Colorados (600 m.a.s.l.), Ecuador. The morphology and geology of this area are influenced by the nearby Andes. The area belongs to a slightly dissected plain in the eastern part of the natural region with a tropical humid to perhumid climate. In this region, the Andes are drained by the rivers Toachi and Baba (not shown in Figure 1).

The allophane layer is believed to consist of altered Quaternary volcanoclastic rocks, although fragments of volcanic origin are rarely found at the surface due to advanced weathering. The thickness of the layer ranges from 5 to 15 m, generally decreasing toward the west. Locally, only minor variation in the thickness is observed, indicating eolian sedimentation of volcanic ash. Vitric and humic Andosols are the dominant soil units on top of this layer (FAO-UNESCO, 1971). The thickness of the underlying sequence (mostly lahars), like the allophane layer, also decreases from east to west, indicating that the material was transported from the Andes toward the west. The volcanic ash was sourced from several volcanoes of intermediate (andesitic) composition. Calculations performed to assess the risk of volcanic eruptions indicate that Guagua Pichincha is probably located too far to the northeast to be considered a source. The ash more likely was sourced from the volcanoes Ninahuilca, Illiniza, or Quilotoa (Figure 1).

MATERIALS AND METHODS

A 16-m profile (termed PM-4) at a recent road-building site was chosen for detailed investigation (Figure 2). Sample collection started at 0.5 m below the surface with sample #PM-4-1. Samples were taken at 1-m intervals down to 16 m (#PM-4-16). The sample name indicates the position in m below the surface.

The samples were air dried, crushed to <2 mm, dried at 40ºC, and ground to <0.25 mm by a hammer mill. The water content was determined by oven drying at 105ºC until constant weight (until no further weight loss was observed).

The samples were analyzed using X-ray fluorescence (XRF), X-ray diffraction (XRD), infrared (IR)

https://doi.org/10.1346/CCMN.2009.0570107 Published online by Cambridge University Press

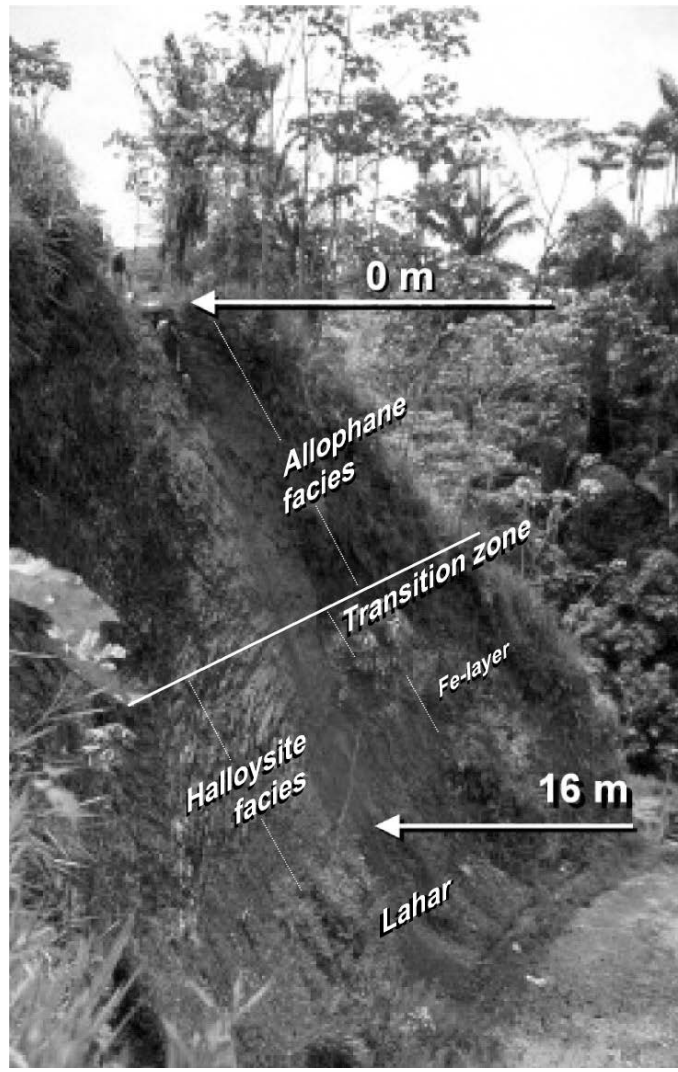

Figure 2. Picture showing the 16-m thick allophane profile which was investigated in detail.

spectroscopy, environmental scanning electron microscopy (ESEM), and carbon analysis (TIC, total inorganic carbon; TOC, total organic carbon; TC, total carbon; and TS, total sulfur) using a LECO oven.

X-ray fluorescence was performed using a PANalytical Axios and a PW2400 spectrometer. The samples were prepared by mixing them with a flux material and melting into glass beads. To determine loss on ignition (LOI) 1000 mg of sample material was heated to 1030ºC for 10 min.

X-ray diffraction patterns were recorded using a Philips X'Pert PW3710 θ-2θ diffractometer (CuKα radiation generated at 40 kV and 40 mA) equipped with a 1º divergence slit, a diffracted-beam monochromator, a scintillation counter, and a sample changer (sample diameter 28 mm). The samples were investigated from 2 to 80º2θ with a step size of 0.02º2θ and a measuring time of 3 s per step. For specimen preparation the top-loading technique was used.

Scanning electron microscopy (SEM) images were recorded using an ESEM FEI Quanta 600 FEG environmental scanning electron microscope in low-vacuum mode.

The specific surface area (SSA) was determined by N_2 adsorption using a 5 point BET method. Measurements were performed using a Micromeritics Gemini III 2375 surface area analyzer with ~300 mg of sample. Prior to measurement, the samples were degassed in vacuum in order to remove adsorbed water.

The organic carbon (OC) content was measured using a LECO CS-444-Analyzer after dissolution of the carbonates. Carbonates were removed by treating the samples several times at 80ºC with HCl until no further gas evolution was observed. Samples of 170−180 mg of

https://doi.org/10.1346/CCMN.2009.0570107 Published online by Cambridge University Press

the dried material were used to measure the total carbon (TC) content.

For the atomic force microscopy (AFM) investigation, individual allophane particles were immobilized on mica as follows: 1 mg of the allophane sample was dispersed in 10 mL of water, followed by ultrasonic treatment for 10 min. The suspension was centrifuged at 4500 rpm for 10 min. 20 μL of the supernatant were dropped on a freshly cleaved, round mica plate (diameter: 15 mm) and finally dried at 60ºC. For investigation by AFM, a multimode AFM from DI in combination with a Nanscope-IIIa-controller was operated in intermittent contact mode using a cantilever (NSC 36/A from MikroMash) with a typical force constant of 0.95 N/m and a tip with a radius of curvature of r <10 nm.

Bulk-soil organic matter of two samples (PM-4-5 and PM-4-10) was taken for radiocarbon dating. The radiocarbon dates were determined by conventional gas counters. Six weeks after preparation of the counting gas, the acetylene ^{14}C activity was recorded.

To measure mid and far infrared (MIR, FIR) spectra, the KBr pellet technique (1 mg of sample/200 mg of KBr) was applied. Spectra with a resolution of 2 cm^{-1} were collected using a Thermo Nicolet Nexus FTIR spectrometer (MIR: beam splitter: KBr, detector DTGS TEC; FIR: beam splitter: solid substrate, detector DTGS PE).

The Al/Si ratio of the allophane was determined by three different methods because of known strengths and weaknesses of the individual methods (which are discussed in detail in the following section). Method 1 is based on ammonium oxalate and pyrophosphate extraction (Blakemore *et al.*, 1981) and conversion of the data according to Harsh *et al.* (2002). For method 2, XRF data of purified fractions (purified by centrifugation) were used; and for method 3, SEM-EDX analyses of apparently pure allophane aggregates were performed.

RESULTS AND DISCUSSION

Chemical composition

The chemical composition of major oxides and trace elements were determined (Table 1) and, based on XRF data, an Fe-rich layer was identified at a depth of 12−13 m. The corresponding values are given in italics (Table 1). This layer is of particular interest because it might be used as a marker horizon to correlate stratigraphically different vertical sequences within the allophane-bearing area. The LOI follows a bimodal distribution, with a transition zone between depths of 9 and 10 m. It decreases with depth from 24−25 wt.% in the upper part of the profile, down to 15−16 wt.% in the lower part. MgO, CaO, Na_2O, and K_2O follow the same trend as the LOI, with significantly more in the upper than in the lower part. In contrast, Al_2O_3 increases gradually with depth, interrupted only by the large Fe_2O_3 contents of the Fe-rich layer. The SiO_2 content varies unsystematically. The trace-element composition reveals no striking features except that As is enriched in the Fe-rich layer, which can be explained by the accumulation of AsO_4^{3-} on Fe-oxyhydroxide surfaces.

The XRF results indicated the presence of two different facies separated by a 2-m thick transition zone.

Mineralogical composition

The facies differentiation, as indicated by XRF, is confirmed by XRD. According to the main mineral components, the upper part was termed 'allophane facies' and the lower part 'halloysite facies' (Figure 2, Table 2). Characteristic minor components of the 'allophane facies' are hornblende and feldspar, which are absent from the 'halloysite facies.' In previous studies (Zeisig *et al.*, 2004, 2005; Kaufhold *et al.*, 2007a, 2007b), the weak XRD intensity at ~14 Å was

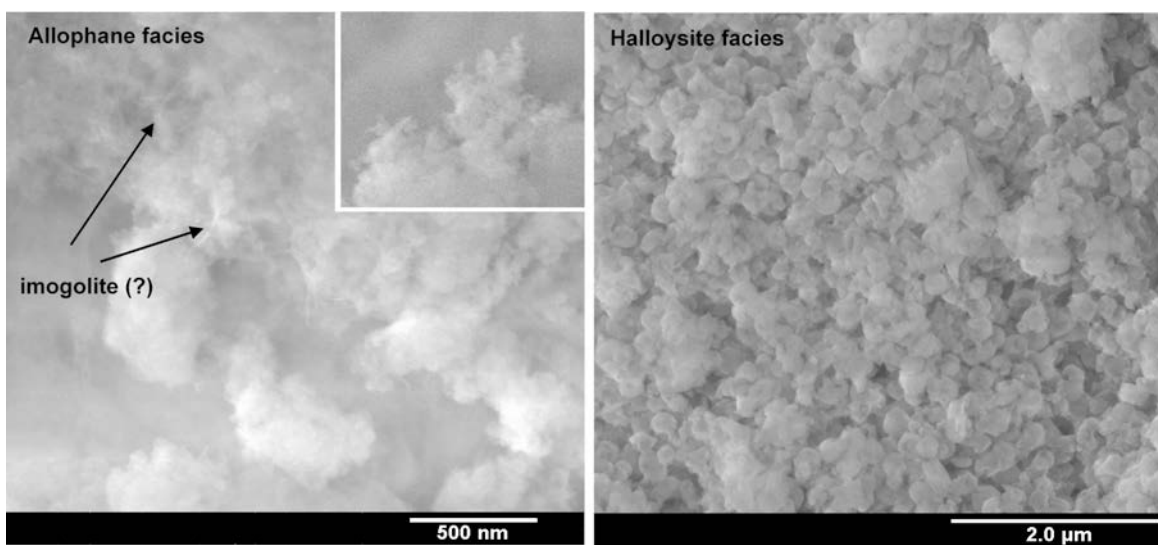

Figure 3. SEM image of the allophane and halloysite facies.

https://doi.org/10.1346/CCMN.2009.0570107 Published online by Cambridge University Press

Table 1. Chemical composition as determined by XRF (major oxides (wt.%) and trace elements (ppm)).

Sample	PM-	4-1	4-2	4-3	4-4	4-5	4-6	4-7	4-8	4-9	4-10	4-11	4-12	4-13	4-14	4-15	4-16
Depths	(m)	0.5	1.5	2	3	4	5	6	7	8	9	10	11	12	13	14	14.5
SiO_2		41.5	39.1	38.0	38.0	34.6	31.8	37.9	31.2	33.4	36.4	37.9	42.8	31.9	31.9	42.8	44.7
TiO_2		0.8	0.9	0.9	0.8	1.0	0.9	0.8	1.0	1.1	1.0	1.0	1.0	0.8	0.9	1.2	1.3
Al_2O_3		22.7	24.9	24.2	23.5	25.7	26.3	25.8	29.3	28.6	30.2	28.0	31.4	24.9	24.7	30.8	32.5
Fe_2O_3		8.4	7.3	9.0	9.8	9.9	9.7	7.2	12.3	11.8	10.6	11.4	8.4	26.0	26.2	9.5	5.8
MnO		0.1	0.1	0.1	0.1	0.1	0.1	0.1	0.1	0.2	0.1	0.2	0.0	0.0	0.0	0.0	0.0
MgO		2.5	1.6	2.1	3.5	1.9	1.2	2.2	0.5	0.5	0.8	1.2	0.1	0.1	0.0	0.0	0.1
CaO		2.7	1.3	1.7	2.5	1.2	0.7	1.4	0.3	0.4	0.6	0.8	0.1	0.1	0.1	0.1	0.1
Na_2O		1.4	0.7	0.8	0.9	0.4	0.2	0.5	0.1	0.1	0.1	0.2	0.1	0.0	0.0	0.1	0.1
K_2O		0.4	0.3	0.2	0.2	0.1	0.1	0.2	0.1	0.0	0.0	0.1	0.1	0.0	0.0	0.0	0.0
P_2O_5		0.1	0.1	0.1	0.1	0.1	0.1	0.0	0.0	0.0	0.0	0.0	0.0	0.0	0.0	0.0	0.0
LOI		18.9	23.3	22.6	20.2	24.6	28.7	23.5	24.5	23.3	19.4	18.6	15.5	15.6	15.4	14.8	14.9
Sum		99.6	99.6	99.6	99.6	99.6	99.6	99.6	99.4	99.4	99.4	99.4	99.5	99.5	99.3	99.4	99.4
As		5	7	5	<2	5	4	5	6	6	2	4	6	15	12	5	<2
Ba		379	348	199	115	112	111	84	590	683	841	681	972	830	1337	1864	1911
Bi		<3	<3	<3	<3	<3	<3	<3	<3	<3	<3	<3	5	4	<3	<3	<3
Ce		25	62	27	31	58	50	82	101	79	22	74	<20	<20	84	45	<20
Co		22	14	12	26	17	20	27	33	54	29	51	17	18	30	33	26
Cr		38	39	42	74	53	60	76	60	84	75	73	42	83	140	94	79
Cs		<5	<5	<5	<5	6	6	<5	6	<5	<5	6	<5	6	<5	7	8
Cu		37	34	33	20	49	56	26	129	80	81	76	80	65	71	50	43
Ga		26	31	31	25	33	30	28	33	35	34	33	37	28	25	40	39
Hf		5	<5	5	<5	10	7	8	7	6	<5	<5	<5	9	<5	<5	7
La		<20	20	23	<20	<20	<20	<20	<20	<20	20	28	38	32	<20	<20	33
Mo		<2	<2	5	<2	<2	<2	<2	<2	<2	<2	<2	3	4	4	<2	3
Nb		3	13	8	3	6	13	8	8	7	6	5	11	24	6	5	8
Nd		<50	55	<50	<50	<50	<50	<50	<50	56	<50	<50	<50	<50	<50	<50	<50
Ni		18	15	13	30	16	13	15	46	47	75	51	55	14	57	72	63
Pb		10	13	10	7	10	13	13	10	7	8	11	19	6	13	6	13
Pr		<50	<50	<50	<50	<50	<50	<50	<50	<50	<50	<50	<50	<50	<50	<50	<50
Rb		11	11	9	8	5	7	10	5	5	<2	5	6	5	3	6	10
Sb		<5	<5	<5	<5	<5	<5	<5	<5	<5	<5	<5	<5	<5	5	<5	<5
Sc		16	16	17	21	20	18	17	16	22	17	15	14	30	25	26	17
Sm		<50	<50	<50	<50	<50	<50	<50	<50	<50	<50	<50	<50	<50	<50	<50	<50
Sn		4	<2	<2	<2	2	4	2	3	2	4	6	<2	4	<2	<2	3
Sr		184	114	109	140	56	33	63	63	74	62	48	38	23	25	32	33
Ta		<5	<5	<5	<5	<5	<5	<5	<5	<5	<5	<5	<5	<5	<5	<5	<5
Th		8	11	11	<5	11	18	14	6	<5	<5	<5	18	18	<5	6	10
U		3	8	8	5	5	14	5	5	8	<3	4	4	9	7	<3	8
V		183	175	190	226	227	193	147	213	245	248	248	212	238	264	241	184
W		<5	<5	<5	<5	<5	<5	<5	<5	<5	<5	<5	<5	<5	<5	<5	<5
Y		7	9	<3	4	10	6	4	<3	<3	<3	<3	6	<3	<3	3	<3
Zn		91	63	71	92	67	49	64	64	73	91	107	111	108	141	144	129
Zr		136	196	168	111	166	218	176	201	172	169	168	218	309	138	164	196

considered to be of vermiculite, though its presence in the present study could not be proved unambiguously. Gibbsite only appears in the transition zone between the two facies. In contrast, hornblende, for example, provides a sharp facies border. The same holds true for the specific surface area (SSA), which decreases significantly at the facies border. The greatest SSA value was found at a depth of 5 m, probably indicating the greatest allophane concentration.

Allophane contents are commonly determined by extraction techniques which, using standard conditions, may not lead to complete dissolution of allophane as a result of its high concentration (Dohrmann *et al.*, 2002). Use of a special XRD Rietveld technique based on the addition of an internal standard and subsequent comparison of original and oxalate-treated samples was suggested by Dohrmann *et al.* (2002). The amounts of XRD-amorphous components were quantified and the results were crosschecked with chemical analyses. Using this Rietveld technique, Dohrmann *et al.* (2002) identified undissolved XRD-amorphous components which correlated well with the chemical balance calculations; these components resulted in an allophane (+imogolite) content of ~80 wt.% for sample PM-4-6. The XRD technique will be discussed in detail in a separate study.

https://doi.org/10.1346/CCMN.2009.0570107 Published online by Cambridge University Press

Table 2. Qualitative mineralogical composition, specific surface area determined by N_2-BET, and TOC.

	Allophane facies									Halloysite facies						
Sample PM-	4-1	4-2	4-3	4-4	4-5	4-6	4-7	4-8	4-9	4-10	4-11	4-12	4-13	4-14	4-15	4-16
Depths (m)	0.5	1.5	2	3	4	5	6	7	8	9	10	11	12	13	14	14.5
X-ray amorphous (allophane, ±imogolite (?) ±Fe oxides (?))	+	+	+	+	+	+	+	+	+	+	+	+–	+–	+–	+–	+–
Halloysite								+	+	+	+	+	+	+	+	+
Gibbsite	–							–	–	+–	–	–				
Quartz	–	–	–	–	–	–	–	–	–	–	–	–	–	–	–	–
Cristobalite	–	–	–	–	–	–	–	–	–	–	–	–	–	–	–	–
Hornblende	+–	–	–	–	–	–	+–	–	–	–	–					
Feldspar	+–	+–	+–	+–	–	–	–									
Goethite	–	–	–		–	–	–	+–	+–	+–	–	+–	+	+	–	+–
Magnetite	–	–	–	–	–	–	–			–	–					
Dolomite	–			–												
Ilmenite	–		–	–	–	–		–	–	–	–	–	–	–	–	–
Anatase												–		–	–	–
Specific surface area (BET) (m^2/g)	187	251	225	224	293	325	273	295	294	165	168	64	83	73	54	55
Organic carbon content (TOC, LECO) (wt.%)	1.3	1.4	1.2	0.8	1.0	0.9	0.7	0.4	0.4	0.3	0.2	0.1	0.1	0.1	0.1	0.0

+: main component; +–: minor component; –: trace)

As expected, the organic carbon content is greater at the top of the vertical sequence. Compared to common Andsols, however, even the values measured at the top of the vertical sequence (at a depth of 0.5 m) are small.

Radiocarbon dating

Both the chemical and mineralogical methods revealed the presence of two facies, for which multiple explanatory hypotheses have emerged. One hypothesis suggests that the existence of the two facies can be explained by two volcanic ash layers of different ages (*i.e.* from different eruptions). This model could not be confirmed by radiocarbon age determination. The sample taken from 10 m below the surface (PM-4-10) has a TOC content of 0.3 wt.%. A radiocarbon age of 15,700±880 BP was determined, correlating with a calibrated ^{14}C age of BC 17,760−15,830. This ^{14}C age should be interpreted with care, though, given the small organic content which is near the lower limit of the conventional radiocarbon system. An age underestimation following contamination with younger C is likely. The uppermost sample, taken 5 m below the surface (PM-4-5) has a TOC content of 1 wt.% and gave a radiocarbon age of 20,060±400 BP. Radiocarbon dating of organic matter from soils yields reliable results for the time of burial of A horizons with a carbon concentration exceeding a few percent (Geyh, 2005). In allophane-rich deposits, ^{14}C results are supposed to reflect the mode and intensity of vertical carbon transport rather than the time of soil genesis, which might be the reason for the age inversion of the two samples. Unfortunately, radiocarbon dating did not allow chronological distinction between the two volcanic ash layers.

SEM observations

Allophane is commonly accompanied by varying amounts of imogolite (e.g. Wada, 1989). Imogolite, when occurring in appreciable amounts, can be detected by XRD. In case of the Ecuadorian allophane, the amount of imogolite present was below the detection limit of XRD. A few fibers, supposedly of imogolite, were observed using SEM (Figure 3).

The SEM images of samples from the allophane facies are dominated by aggregates appearing as clouds (Figure 3, left). The diameter of these aggregates is 0.5−1 μm. They consist of millions of primary allophane particles, but their primary particle sizes are less than the resolution of the SEM. In the halloysite facies, more crystalline particles with a diameter of ~0.5 μm were observed (Figure 3, right).

Atomic force microscopy

Atomic force microscopy was applied in order to investigate the primary allophane particles (Figure 4). Next to some isolated allophane particles, some aggregates (two or three adjacent primary particles) were observed, indicating the high affinity of allophane surfaces for each other (Figure 4, top left); this is probably the reason for: (1) the existence of the cloud-like aggregates; and (2) the poor dispersibility (Harsh, 2000; Kaufhold *et al.*, 2007b).

https://doi.org/10.1346/CCMN.2009.0570107 Published online by Cambridge University Press

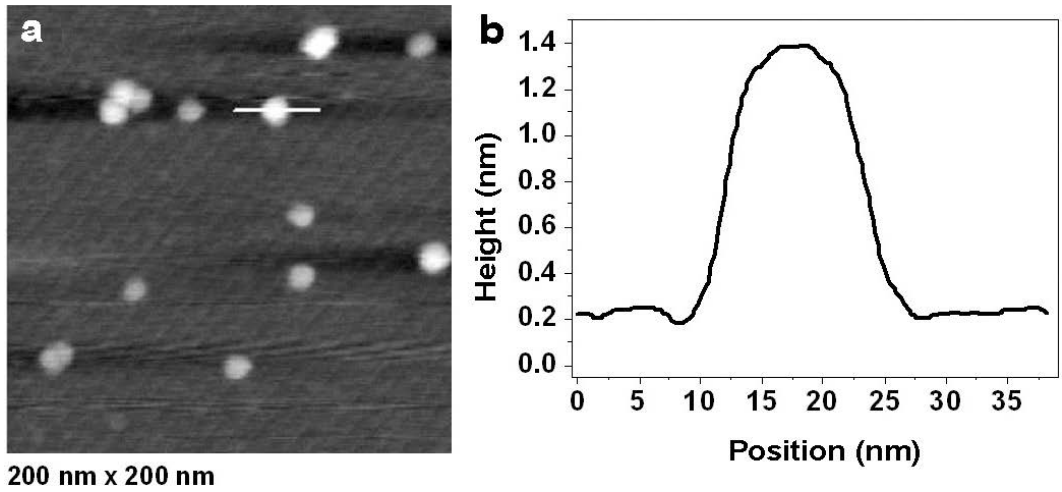

Figure 4. (a) AFM topography image of some individual allophane primary particles and small particle aggregates; and (b) the cross section of an allophane particle along the white bar.

The diameter of the primary allophane particles is known to range from 3 to 5 nm (Henmi & Wada, 1976; van der Gaast *et al.*, 1985, Wada, 1989). The AFM profile (Figure 4b) is consistent with a particle diameter of 15 nm. As the apex radius of the AFM tip used is between 5 and 10 nm and thus has a dimension which is comparable to that of the allophane primary particles, the possibility of tip convolution has to be taken into account. The geometrical conditions of tip convolution show that the size of the particles (with a real, average diameter of 4 nm), which is measured using an AFM tip with an average apex radius of 7 nm, would be 15 nm if an ideal spherical shape of the particles is assumed. The cross section (Figure 4b) shows that the measured height of the particle is ~1.3 nm, which is smaller than the expected height (or diameter) of allophane particles. Accordingly a flattening of the particle shape owing to the strong interaction between the mica substrate and the particles cannot be excluded. Taking into account the geometrical conditions described above and summarizing the results of the AFM investigation, a real diameter of the particles (Figure 4a) ranging from 3 to 5 nm is probable, as is reported in the literature (even if a flattening of the particles occurs during adsorption).

Infrared spectroscopy

The main IR vibration of Al-rich allophanes is located between 975 cm^{-1} (Al/Si = 2) and 1020 cm^{-1} (Al/Si = 1) (Parfitt, 1990). The main vibration of the allophane-rich sample, PM-4-6, is located at 1005 cm^{-1} (Figure 5) suggesting an Al/Si ratio of ~1.3 (according to Parfitt, 1990), which is in good agreement with average values determined by Dohrmann *et al.* (2002).

The spectrum of sample PM-4-11 is dominated by halloysite, which can be distinguished from disordered kaolinite by the presence of only two bands in the

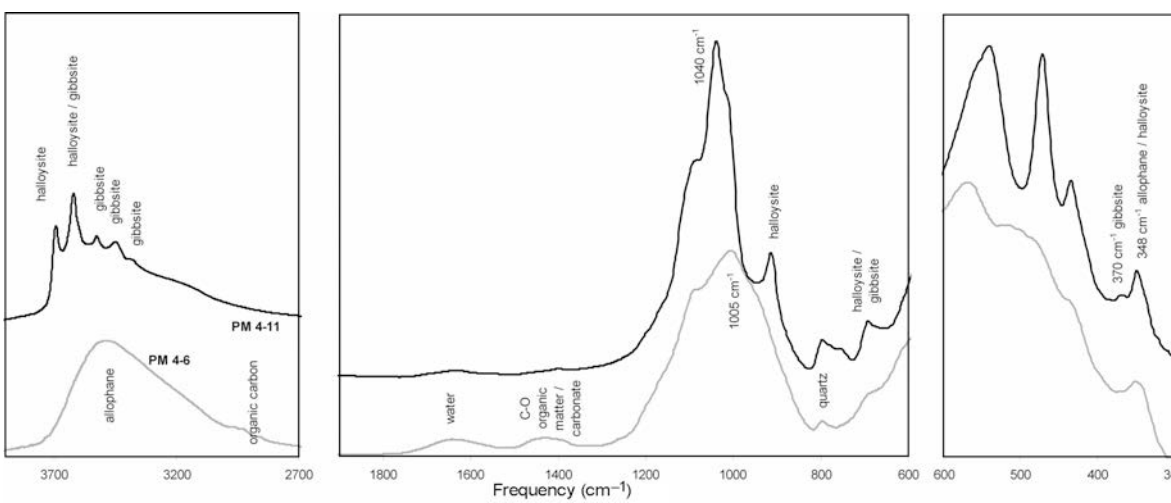

Figure 5. FIR and MIR spectra of samples PM-4-6 (allophane facies) and PM-4-11 (halloysite facies).

https://doi.org/10.1346/CCMN.2009.0570107 Published online by Cambridge University Press

OH-stretching region (3600−3700 cm^{-1}). In addition, the presence of quartz and gibbsite, as determined by XRD, was confirmed. No information can be gained about minor amounts of allophane possibly present in sample PM-4-11 because minor amounts of allophane can be masked by the halloysite bands. The most characteristic IR band of allophane is located at 348 cm^{-1}. This band, however, can only be assigned to allophane if illite, montmorillonite, kaolinite, and halloysite are absent (Farmer *et al.*, 1977). Neither XRD nor MIR provided evidence for the occurrence of any of these minerals in sample PM-4-6. The 348 cm^{-1} band of sample PM-4-6, therefore, could be assigned to allophane. In the case of sample PM-4-11, this band was assigned mainly to halloysite.

Al/Si ratio/allophane classification

Allophanes are classified by their Al/Si ratio. According to this ratio, allophanes vary in terms of their structure and charge. Infrared spectroscopy provided an estimated Al/Si ratio of 1.3. More accurate values for the Al/Si ratio can be obtained by extraction techniques (Blakemore *et al.*, 1981). Based on the calculation suggested by Harsh *et al.* (2002), an average Al/Si molar ratio of 1.4 was found within the allophane facies. This was confirmed by EDX analysis of 20 cloud-like allophane aggregates of sample PM-4-6 (Al/Si = 1.3±0.1; Figure 6). The cloud-like allophane aggregates contained appreciable amounts of Fe. No indication of the presence of separate Fe phases was found in the SEM images. In addition, the Al/Fe molar ratio shows strong variation compared to the Al/Si molar ratio. This indicates that Fe is present as a separate phase but obviously finely dispersed within the cloud-like allophane aggregates.

By XRF analysis of the <0.2 μm fraction, an Al/Si molar ratio of 1.2 was determined. The XRD analysis of this fraction proved the presence of minor amounts of cristobalite and quartz, which explains the slightly smaller value.

Different methods gave Al/Si ratios for the Ecuadorian allophane ranging from 1.3 to 1.4. Such allophanes are referred to as 'stream deposit allophanes' or as 'silica springs allophane' (Parfitt, 1990) and represent an intermediate between the Al-rich soil allophanes (Al/Si = 2: proto-imogolite allophane or imogolite-like allophane) and the Si-rich allophanes (Al/Si = 1: pumice allophane or halloysite-like allophane). According to Wells *et al.* (1977) the stream deposit allophanes found in New-Zealand have a diameter of <3 nm. Considering the Al/Si molar ratio, the Ecuadorian allophane clearly has to be classified as a stream deposit or as silica springs allophane. In contrast to this type of allophane, known from New Zealand, the primary allophane particle size from Ecuador seems to be larger.

SUMMARY AND CONCLUSIONS

A very large allophane deposit north and west of Santo Domingo de los Colorades (Ecuador) is described. Mineralogical and geochemical results indicate the presence of two volcanic ash layers differing both in terms of composition and age. The latter could not be proved by the ^{14}C method probably because the TOC content was too small. The age of the allophane-rich layer is ~20,000 years BC.

Different mineralogical and chemical compositions suggest that the two facies contain ashes of two different volcanic eruptions. The halloysite facies may contain

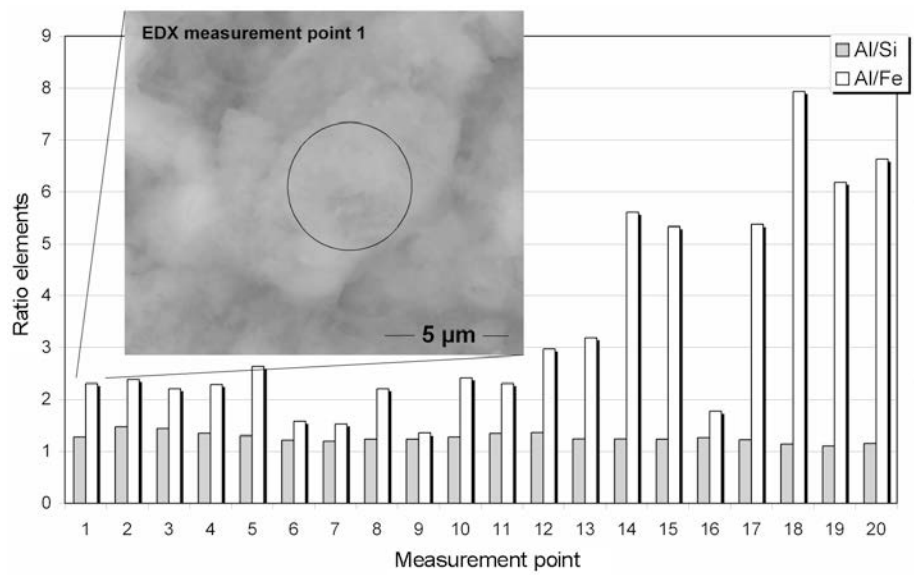

Figure 6. Al/Si and Al/Fe molar ratios determined by EDX measurements (the image depicts measurement point 1).

https://doi.org/10.1346/CCMN.2009.0570107 Published online by Cambridge University Press

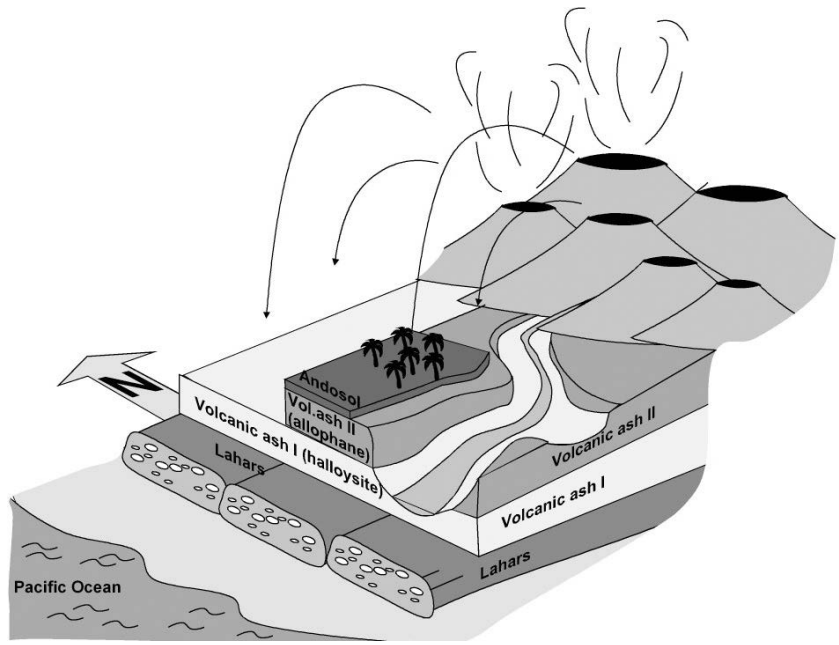

Figure 7. Idealized sketch of the geological setting of the allophane-rich layer.

volcanoclastic material that was weathered extensively in contrast to the volcanoclastic material from the allophane facies which is considered to be in an ongoing weathering and mineral-alteration process, as indicated by the concentration gradient of the alkali earth metals, probably reflecting different degrees of weathering and leaching.

The Al/Si ratio of the allophane is ~1.3 corresponding to so-called stream-deposit allophanes (Parfitt, 1990). A schematic representation of the geological setting and current model of the formation of the allophane deposit (Figure 7) reveal that the altered volcanic ash layers (allophane and halloysite) overly a layer of lahars and the morphology is influenced by recent fluvial erosion.

The allophane raw material is currently being tested for various industrial applications and the massive, high-quality deposit could be the basis for low-cost nano-materials with many applications yet to be discovered. Therefore, different purification techniques and the irreversible effect of drying are currently being investigated in detail. Future studies will be devoted to the mechanism of formation of the allophane layer and its lateral homogeneity. Finally, the exact location of Fe within the allophane structure and/or cloud-like aggregates should be investigated using Mössbauer spectroscopy.

REFERENCES

Benbow, J. (1990) New Zealand's minerals for domestic consumption. *Industrial Minerals*, **273**, 19–35.

Blakemore, L.C., Searle, P.L., and Daly, B.K. (1981) *Methods for Chemical Analysis of Soils*. New Zealand Soil Bureau, Department of Scientific and Industrial Research, Report 10A, New Zealand.

Dohrmann, R., Meyer, I., Kaufhold, S., Jahn, R., Kleber M., and Kasbohm, J. (2002) Rietveld based-quantification of allophane. *Mainzer Naturwissenschaftliches Archiv*, **40**, 28–30.

FAO-UNESCO (1971) Soil map of the world 1:5,000,000. Vol. IV – South America. Paris.

Farmer, V.C., Fraser, A.R., Russell, J.D., and Yoshinaga, N. (1977) Recognition of imogolite structures in allophanic clay by infrared spectroscopy. *Clay Minerals*, **12**, 55–57.

Geyh, M.A. (2005): ^{14}C dating – still a challenge for users? *Zeitschrift für Geomorphologie N.F.*, **139,** 63–86.

Harsh, J. (2000) Poorly crystalline aluminosilicate clays. Pp. F169–F182 in: *Handbook of Soil Science* (M.E. Sumner, editor). CRC Press, Boca Raton, Florida, USA.

Harsh, J., Chorover, J., and Nizeyimana, E. (2002) Allophane and Imogolite. Pp. 291–322 in: *Soil Mineralogy with Environmental Applications* (W.A. Dick, editor). Soil Science Society of America, Madison, Wisconsin, USA.

Henmi, T. and Wada, K., (1976) Morphology and composition of allophane. *American Mineralogist*, **61**, 379–390.

Kaufhold, S. (2007) Ecuadorian Allophane. *Industrial Minerals*, May 2007, p. 95.

Kaufhold, S., Zeisig, A., Jahn, R., Dohrmann, R., and Brito, S. (2007a) Allophane from Ecuador. *CMS Annual meeting in Santa Fe, Program and abstracts*, p. 108. Available online at: http://www.sandia.gov/clay/docs/CMS_Program.pdf.

Kaufhold, A., Dohrmann, R., and Jahn, R. (2007b) *Einfluss der Trocknung auf die Eigenschaften von Allophan*. DBG Mitteilungen, **110**, No. 2, ISSN 0343-1071, pp. 647–648.

Parfitt, R.L. (1990) Allophane in New Zealand – A Review. *Australian Journal of Soil Research*, **28**, 343–360.

van der Gaast, S.J., Wada, K., Wada, S.I., and Kakuto, Y. (1985) Small-angle X-ray powder diffraction, morphology, and structure of allophane and imogolite. *Clays and Clay Minerals*, **33**, 237–243.

Wada, K. (1989) Allophane and imogolite. Pp. 1051–1087 in: *Minerals in Soil Environments* (J.B. Dixon and S.B. Weed,

https://doi.org/10.1346/CCMN.2009.0570107 Published online by Cambridge University Press

editors). Soil Science Society of America, Madison, Wisconsin, USA.

Wells, N., Childs, C.W., and Downes, C.J. (1977) Silica springs, Tongariro national park, New Zealand – analyses of the spring water and characterization of the alumino-silicate deposit. *Geochmica et Cosmochimica Acta*, **41**, 1497–1506.

Yuan, G. (2004) Environmental nanomaterials: Occurrence, syntheses, characterization, health effect, and potential applications. *Journal of Environmental Science and Health, Part A – Toxic/Hazardous Substances & Environmental Engineering*, **A39**, 2545–2548.

Zeisig, A., Schöneich, S., Kaufhold, S., Dohrmann, R., and Jahn, R. (2004) Allophanreicher Ton - ein 'special clay' aus Ecuador. Pp. 103–104 in: *Berichte der DTTG*, **10**, (R. Nüesch and K. Emmerich, editors). Karlsruhe, ISSN 1432-7007, available online at http://www.dttg.ethz.ch/vol10_dttg2004.pdf.

Zeisig, A., Jahn, R., Dohrmann, R. and Kaufhold, S. (2005) Allophane rich clay – a special clay from Santo Domingo de los Colorados/Ecuador, characterisation and potential application. Pp. 99–104 in: *Berichte der DTTG, Celle*, **11** (R. Dohrmann and S. Kaufhold, editors). ISSN 1432-7007, available online at http://www.dttg.ethz.ch/vol11_dttg2005.pdf.

(*Received 29 April 2008; revised 24 September 2008; Ms. 0155; A.E. J.D. Fabris*)